The Astronomical Journal, 125:785–793, 2003 February

CHAOS CAUSED BY RESONANCE OVERLAP IN THE SOLAR NEIGHBORHOOD: SPIRAL STRUCTURE AT THE BAR'S OUTER LINDBLAD RESONANCE

A. C. Quillen[1]
Department of Physics and Astronomy, University of Rochester, 600 Wilson Boulevard, Rochester, NY 14627-0171; aquillen@pas.rochester.edu
Received 2002 April 8; accepted 2002 October 17

ABSTRACT

We consider the nature of orbits near the solar neighborhood that are perturbed by local spiral arms and the Milky Way bar. We present a simplified Hamiltonian model that includes resonant terms from both types of perturbations and is similar to the forced pendulum. Via numerical integration of this model, we construct Poincaré maps to illustrate the nature and stability of the phase space. We find that resonance overlap is most likely to cause widespread chaos when the pattern of the spiral structure puts the solar neighborhood near the 2 : 1 inner Lindblad resonance (ILR) in the case of a two-armed pattern, or near the 4 : 1 ILR in the case of a four-armed pattern. When this happens, both the quasi-periodic orbits that support the spiral structure and those that oscillate with the bar are disrupted near the bar's 2 : 1 outer Lindblad resonance (OLR). Consequently, the pattern speed of spiral structure that passes through the bar's OLR must be faster than $\sim$0.45 times the solar neighborhood angular rotation rate if it is two-armed, or faster than 0.75 times this value if it is four-armed. Alternatively, the bar's OLR may form a boundary between spiral modes at different pattern speeds. In all cases, we find that spiral structure is disrupted by the bar's OLR over a narrow range of radius, and that the extent of the orbits aligned perpendicular to the bar at the bar's OLR is limited by the spiral perturbations. We find that the boundary, at an azimuthal velocity component of 30 km s^{-1} below that of the Sun, of the *u*-anomaly in the velocity distribution in the solar neighborhood is due to the abrupt bifurcation of the orbit families associated with the OLR. The upper boundary at 60 km s^{-1} is truncated by the spiral structure. The radial velocity width of the anomaly is probably bounded by chaotic regions that surround the family of quasi-periodic orbits oriented perpendicular to the bar.

Key words: Galaxy: kinematics and dynamics — solar neighborhood

1. INTRODUCTION

It has been established, beyond doubt, that the Milky Way is barred, as are many nearby galaxies. Evidence for the bar comes from asymmetry in the bulge surface photometry, star counts, and interpretation of the gas kinematics (for a recent review, see Gerhard 2002). The most common values suggested from these observations are a co-rotation radius of 3.5–5 kpc and a major-axis in-plane angle with respect to the Galactic center of $\phi_{\rm bar} \sim 15^\circ$–$45^\circ$.

The solar neighborhood local velocity distribution is expected to contain structure caused by large-scale, nearby gravitational perturbations. While structure at velocities near that of the Sun is likely to be affected by spiral structure and disrupted stellar clusters (see, e.g., Skuljan, Hearnshaw, & Cottrell 1999), the Hercules Stream, with tangential velocity component 45 km s^{-1} below that of a star in a circular orbit at the Galactic radius of the Sun, is suspected to be related to the 2 : 1 outer Lindblad resonance (OLR) with the Galactic bar (Dehnen 1999; Fux 2001; Raboud et al. 1998). This stream is also known as the *u*-anomaly. Because of the older stars in it, the stream probably has a stable kinematic origin (Raboud et al. 1998; Dehnen 1998). The local velocity distribution as constructed from the *Hipparcos* Catalogue most clearly shows this stream as a strong and separate feature (Dehnen 1998); in fact, there is a saddle point in the distribution between the stream and the bulk of the stars at $v \sim 30$ km s^{-1} (see figures in Dehnen 1998 and Fux 2001).

Linear theory predicts that the orientation of orbits will shift across the OLR, from oriented along the bar's major axis outside the OLR to perpendicular to the bar within it (Binney & Tremaine 1987). Near the peak of the resonance, both types of orbits can exist (Contopoulos 1975; Weinberg 1994). Dehnen (2000) showed, using a backward-integrating bar growth model, that stars were likely to be captured into resonant regions associated with these two major orbit families. He found that the resulting velocity distribution was dependent upon the timescale over which the bar was grown in the simulation, as well as the assumed initial velocity distribution. Fux (2001) considered the stability of orbits and suggested that chaotic regions associated with resonances were likely to cause overdensities in some regions of phase space and underdensities in others. He illustrated with *N*-body simulations that the resulting stellar distribution could correspond to that observed.

In some sense, it is surprising that the OLR with the bar provides such a good explanation for the *u*-anomaly, because locally both gaseous and stellar tracers primarily show spiral structure near the solar circle (see, e.g., Vallée 1995; Drimmel & Spergel 2001). Previous works have not considered the more complicated problem caused by the forces due to local spiral structure in addition to those caused by the bar.

In this paper, we consider the dynamics of stars that are affected by perturbations from both spiral structure and the Milky Way bar. We construct a simple Hamiltonian model for the dynamics that contains resonant terms at both the bar's pattern speed and a slower pattern speed from local spiral structure. We find that the Hamiltonian can exhibit

[1] Visitor, Department of Physics, Technion, Israel Institute of Technology.

resonance overlap and so wide-scale chaos. Consequently, we address the issue of orbit stability by computing area-preserving, or Poincaré, maps for different values of the spiral pattern speed.

2. HAMILTONIAN FORMALISM FOR THE KINEMATICS

As shown by Contopoulos (1975, 1988), the dynamics of stars confined to the Galactic plane moving in a smooth Galactic potential lacking nonaxisymmetric perturbations is described by a Hamiltonian that can be written in a third-order post-epicyclic approximation as

$$H_0(I_1,\theta_1;I_2,\theta_2) = h + \omega_1 I_1 + \omega_2 I_2 + aI_1^2 + 2bI_1I_2 + cI_2^2 + \cdots . \quad (1)$$

The high order of the expansion is required to exhibit the bifurcation of the major resonances.[2] The action variables $I_1 = (2\pi)^{-1}\int \dot{r}\, dr$ and $I_2 = J_0 - J_c$ are integrals of the motion when the Hamiltonian is unperturbed. The quantity J_0 is the particle's angular momentum, and J_c is the angular momentum of a particle in a circular orbit at a radius r_c, which is the radius of a circular orbit with value h. The frequencies and constants in the above Hamiltonian are evaluated at this radius. We can choose to work in either a frame rotating with a perturbation pattern or an inertial one. Contopoulos (1975) worked in a frame rotating at the bar or spiral pattern speed, Ω_s, so $h \equiv \frac{1}{2}J_c^2/r_c^2 + V_0(r_c) - \Omega_s J_c$ and $\omega_2 = \Omega_c - \Omega_s$, where Ω_c is the angular rotation rate of a circular orbit. Since we will consider more than one perturbation and each perturbation will have a different pattern speed, in this paper we choose to work in an inertial frame. Consequently, $h \equiv \frac{1}{2}J_c^2/r_c^2 + V_0(r_c)$ and $\omega_2 = \Omega_c$. In either frame, $J_c = r_c^2\Omega_c$ is the angular momentum and $V_0(r)$ is the axisymmetric component of the potential. The frequency $\omega_1 = \kappa_c$, where κ_c is the epicyclic frequency, which is evaluated at r_c. Unfortunately, the value of r_c depends on Ω_s, so transferring coordinate systems between an inertial and a rotating one is not trivial.

The constants a, b, and c are given in Appendix A of Contopoulos (1975). When the rotation curve is flat, $\kappa_c = \sqrt{2}\Omega_c$, $a = -0.92/r_c^2$, $b = -1/(\sqrt{2}r_c^2)$, and $c = -1/(2r_c^2)$.

The radius r, the angle θ, and their time derivatives are related to the action angle variables to first order in $I^{1/2}$:

$$r - r_c \approx \left(\frac{2I_1}{\kappa_c}\right)^{1/2}\cos\theta_1 , \quad \frac{dr}{dt} \approx -(2I_1\kappa_c)^{1/2}\sin\theta_1 , \quad (2)$$

$$\theta \approx \theta_2 - \frac{2\Omega_c}{r_c\kappa_c}\left(\frac{2I_1}{\kappa_c}\right)^{1/2}\sin\theta_1 , \quad r^2\frac{d\theta}{dt} \approx I_2 + r_c^2\Omega_c \quad (3)$$

(from Appendix A of Contopoulos 1975), where θ_1 is the epicyclic angle and θ_2 is the azimuth of the epicyclic center. The quantities θ_1 and θ_2 are the angle variables conjugate to I_1 and I_2.

To consider the effect of nonaxisymmetric perturbations in the gravitational potential caused by a bar or spiral structure, we must estimate the strength of these perturbations in terms of the action angle variables described above.

[2] The coordinates used in the above Hamiltonian are based on a post-epicyclic approximation, not a canonical transformation.

We concentrate on the Lindblad resonances for a number of reasons. They are first-order in the amplitude of the perturbation and in $I^{1/2}$ and, so, likely to be strong. The 2 : 1 OLR from the Galactic bar is near the location of the solar neighborhood. Stars on orbits influenced by the spiral's inner Lindblad resonances (ILRs) are required to self-consistently support spiral structure (see, e.g., Contopoulos 1988).

2.1. *Perturbation from the Milky Way Bar*

For a barlike perturbation, we assume that the nonaxisymmetric component of the gravitational potential depends on radius and can be expanded in Fourier components:

$$V_1(r,\theta) = \sum_m B_m(r)\cos\left[m(\theta - \Omega_b t)\right] , \quad (4)$$

where Ω_b is the angular rotation rate of the bar. In action angle variables, we can write the potential perturbations to first order in $I_1^{1/2}$ and the strength of the perturbation:

$$V_{1,m}(I_1,\theta_1;I_2,\theta_2) = (2I_1/\kappa_c)^{1/2}\beta_m\{\cos\left[\theta_1 + m(\theta_2 - \Omega_b t)\right] + \cos\left[\theta_1 - m(\theta_2 - \Omega_b t)\right]\} \quad (5)$$

(following expressions given by Contopoulos 1988), where the first and second angular terms correspond to the $m:1$ outer and inner Lindblad resonances, respectively. Here

$$\beta_m = \frac{1}{2}B_m' + \frac{m\Omega_c}{r_c\kappa_c}B_m , \quad (6)$$

where B_m and $B_m' = dB_m/dr$ are evaluated at r_c.

The solar neighborhood is well past the end of the Galactic bar, so we can approximate the potential perturbation as a quadrupolar term in the gravitational potential:

$$B_2(r) \approx -a_b(r_b/r)^3 , \quad (7)$$

where r_b is the radius at which the bar ends, $r_b \approx 0.45r_0$, as found from infrared photometry (e.g., Dwek et al. 1995), with r_0 the radius of the solar circle from the Galactic center. The pattern speed of the bar is constrained by to be about 1.85 times the solar neighborhood value of the angular rotation rate, Ω_0 (Dehnen 1999). Fux (2001) considered bars about twice as strong as those considered by Dehnen (1999).

Dehnen (2000) estimates $\alpha = (3a_b/v_c^2)(r_b/r_c)^3 \approx 0.01$, so at the solar circle $a_b/v_c^2 \sim 0.036$. From equation (6), and assuming that the rotation curve is flat, we find $\beta_2 \sim 0.086(a_b/r_c)(r_b/r_c)^3$, so at the solar neighborhood we estimate

$$\beta_2 \sim 0.0003v_c^2/r_c , \quad (8)$$

where v_c is the velocity of a star in a circular orbit.

2.2. *Perturbation from Local Spiral Structure*

For spiral structure, we assume that the radial variations depend on angle and that the amplitude is nearly constant with radius. The potential perturbation is

$$V_{1,m}(r,\theta) = \mathrm{Re}\left(\sum_m A_m \exp\{i[k_m r - m(\theta - \Omega_s t) + \alpha_m]\}\right) . \quad (9)$$

Here m refers to the number of arms, Ω_s to the spiral pattern speed, k_m to the wavenumber, and α_m to an angular offset.

Contopoulos (1975) showed that to first order in $I_1^{1/2}$, the potential perturbation

$$V_{1,m}(I_1,\theta_1;I_2,\theta_2) = (2I_1/\kappa_c)^{1/2}\epsilon_m\{\cos[\theta_1 - m(\theta_2 - \Omega_s t + \gamma_{m+})] + \cos[\theta_1 + m(\theta_2 - \Omega_s t + \gamma_{m-})]\}\ , \quad (10)$$

where

$$\epsilon_m = \frac{A_m k_m}{2}\left[1 + \left(\frac{2m\Omega_c}{k_m r_c \omega_1}\right)^2\right]^{1/2} \quad (11)$$

for $A_m'/(kA_m) \ll 1$. The angular offsets $\gamma_{m\pm}$ depend on α_m and the wavenumber (see Contopoulos 1975 for expressions).

Tracers of spiral structure in the solar neighborhood suggest that the spiral structure is quite tightly wound (see, e.g., Vallée 1995). In the WKB approximation

$$A_m \sim -2G\Sigma_0 S_m/|k_m|\ , \quad (12)$$

where S_m is the amplitude of the spiral surface density variations divided by the mean surface density (Binney & Tremaine 1987). For a tightly wound structure, we expect that $\epsilon_m \sim A_m k_m/2$ (taking the largest term in eq. [11]). The mean surface density of disk mass in the solar neighborhood is $\Sigma_0 \sim 50\ M_\odot\ \mathrm{pc}^{-2}$ (Holmberg & Flynn 2000), and we use $v_c \sim 220\ \mathrm{km\ s}^{-1}$. A two-armed spiral is seen in the near-infrared *COBE* DIRBE data with pitch angle in the range $p \sim 15.^\circ5$–19° (Drimmel & Spergel 2001), yielding $k_m r_0 = m \cot p$ in the range 5.8–7.2 for $m = 2$. The amplitude of the spiral structure could be as large as $S_m \sim 0.5$–1 (Drimmel & Spergel 2001). We estimate for the solar neighborhood

$$A_m \sim -0.011 v_c^2 S_m \left(\frac{\Sigma_0}{50\ M_\odot\ \mathrm{pc}^{-2}}\right)\left(\frac{v_c}{200\ \mathrm{km\ s}^{-1}}\right)^{-2} \times \left(\frac{r_c}{8\ \mathrm{kpc}}\right)\left(\frac{7}{k_m r_c}\right),$$

$$\epsilon_m \sim -0.036 \frac{v_c^2}{r_c} S_m \left(\frac{\Sigma_0}{50\ M_\odot\ \mathrm{pc}^{-2}}\right)\left(\frac{v_c}{200\ \mathrm{km\ s}^{-1}}\right)^{-2} \times \left(\frac{r_c}{8\ \mathrm{kpc}}\right). \quad (13)$$

The expression for ϵ_m is independent of k_m and primarily depends on the amplitude of the spiral density variation.

3. HAMILTONIAN WITH PERTURBATIONS FROM BOTH SPIRAL STRUCTURE AND THE MILKY WAY BAR

We now take the perturbations due to the bar and spiral arms and add them to the unperturbed Hamiltonian. We have estimated the size of the coefficients β and ϵ for these perturbations in the previous section.

We expect that the 2:1 OLR with the Galactic bar and the 2:1 or 4:1 ILR with local spiral structure will be the strongest resonances near the solar neighborhood. To clarify which pattern is associated with which resonance, we refer to the ILRs with the spiral pattern as ILR_S and the OLR with the bar as OLR_B. So, ignoring all other resonant terms, we can simplify the problem to

$$H = aI_1^2 + 2bI_1I_2 + cI_2^2 + \kappa I_1 + \Omega I_2 + \beta_2(2I_1/\kappa)^{1/2}\cos[\theta_1 + 2(\theta_2 - \Omega_b t)] + \epsilon_m(2I_1/\kappa)^{1/2}\cos[\theta_1 - m(\theta_2 - \Omega_s t) - \gamma] + \cdots\ , \quad (14)$$

where $m = 2$ for the 2:1 ILR_S and $m = 4$ for the 4:1 ILR_S.

We perform a canonical transformation with generating function

$$F_2(J_1,J_2,\theta_1,\theta_2) = J_1[\theta_1 + 2(\theta_2 - \Omega_b t)] + J_2\theta_2\ , \quad (15)$$

obtaining a resonant angle and new momenta

$$\phi = \theta_1 + 2(\theta_2 - \Omega_b t)\ , \quad I_2 = 2J_1 + J_2\ . \quad (16)$$

The quantities $I_1 = J_1$ and θ_2 remain unchanged. Our Hamiltonian becomes

$$H(J_1,\phi;J_2,\theta_2) = a'J_1^2 + 2b'J_1J_2 + cJ_2^2 + \delta J_1 + \Omega J_2 + \beta_2(2J_1/\kappa)^{1/2}\cos\phi + \epsilon_m(2J_1/\kappa)^{1/2}\cos(\phi + \alpha - \gamma)\ , \quad (17)$$

where

$$a' = a + 4b + 4c\ , \quad b' = b + 2c\ , \quad (18)$$

$$\delta = \kappa + 2(\Omega - \Omega_b)\ , \quad (19)$$

$$\alpha = (m\Omega_s + 2\Omega_b)t - (m+2)\theta_2\ . \quad (20)$$

When the rotation curve is flat, $a' = -5.7/r_c^2$. We can approximate $\theta_2 \approx \Omega t$, so that $\alpha \approx \nu t$, where

$$\nu = m\Omega_s + 2\Omega_b - (2+m)\Omega\ . \quad (21)$$

Note that J_2 is a constant of the motion. Ignoring the terms dependent upon J_2, we rewrite our Hamiltonian in a simpler form:

$$H(J_1,\phi) \approx a'J_1^2 + \delta J_1 + \beta_2(2J_1/\kappa)^{1/2}\cos\phi + \epsilon_m(2J_1/\kappa)^{1/2}\cos(\phi + \nu t - \gamma)\ . \quad (22)$$

We rescale lengths by r_c and put time in units of Ω^{-1}. Our rescaled Hamiltonian is

$$h(j_1,\phi)/v_c^2 \approx a'r_c^2[j_1^2 + \bar\delta j_1 + \bar\beta_2 j_1^{1/2}\cos\phi + \bar\epsilon_m j_1^{1/2}\cos(\phi + \bar\nu t' - \gamma)]\ , \quad (23)$$

where $J_1 = r_c^2\Omega j_1$. The unitless coefficients are

$$\bar\delta = \frac{\kappa + 2(\Omega - \Omega_b)}{\Omega a' r_c^2}\ , \quad \bar\beta = \frac{\beta_2 r_c/v_c^2}{a'r_c^2}\sqrt{\frac{2\Omega}{\kappa}}\ , \quad (24)$$

$$\bar\epsilon = \frac{\epsilon_m r_c/v_c^2}{a'r_c^2}\sqrt{\frac{2\Omega}{\kappa}}\ , \quad \bar\nu = \frac{m\Omega_s + 2\Omega_b - (2+m)\Omega}{\Omega}\ . \quad (25)$$

If we included the effect of a nonzero value of J_2, there would be a shift in the value of $\bar\delta$ proportional to J_2 from the term $2b'J_1J_2$ in equation (17).

If we set $\bar\epsilon = 0$ so that there is a bar perturbation but no spiral one, $h = j_1^2 + \bar\delta j_1 + \bar\beta j^{1/2}\cos\phi$. This Hamiltonian is in the same form as the *e-e* resonances discussed in the context of solar system orbital resonances (Murray & Dermott 1999; Borderies & Goldreich 1984). As illustrated

by Murray & Dermott (1999) and Borderies & Goldreich (1984), the resonance bifurcates at a critical value of a parameter that depends on $\bar{\delta}$ and $\bar{\beta}$ (see Fig. 1 below). The resonance has three fixed points when

$$\tfrac{2}{3}\bar{\delta}/\left|\bar{\beta}\right|^{2/3} < -1 \ . \tag{26}$$

One of the fixed points is unstable, and the other two correspond to two resonant stable islands of libration at $\phi = 0$ and $\phi = \pi$. Only one fixed point exists when the above inequality does not hold, and its location is determined by the sign of $\bar{\beta}$. When $\bar{\beta} > 0$, this fixed point is at $\phi = 0$, otherwise it is at $\phi = \pi$.

When $\bar{\beta} = 0$, so that there is a spiral perturbation and no bar, the Hamiltonian can be put in the form $h = j_1^2 + \Delta j_1 + \bar{\epsilon} j^{1/2} \cos \phi'$ with a suitable canonical transformation, where $\Delta = \bar{\delta} + \bar{\nu}/(a' r_c^2) = [\kappa - m(\Omega - \Omega_s)]/(\Omega a' r_c^2)$. In this case, the bifurcation happens when

$$\tfrac{2}{3}\Delta/|\bar{\epsilon}|^{2/3} < -1 \ . \tag{27}$$

The resonance can also be illustrated by Figure 1, but with $\bar{\epsilon}$ replacing $\bar{\beta}$ and Δ replacing $\bar{\delta}$ (see Fig. 1 of Contopoulos 1975).

The distinction between regions with two stable fixed points and those with one fixed point is important when resonances overlap. For this type of Hamiltonian, a separatrix exists only when there are two stable fixed points. Because the period of the orbits becomes infinite at the separatrix, additional perturbations are most likely to cause instability and a chaotic region near the original location of the separatrix. When we have two resonant terms in the Hamiltonian and the resonances overlap, large regions of phase space will become strongly chaotic only when at least one of the resonances contains a separatrix.

We now consider the orientations of the orbits and signs of the individual terms. Fixed points in our simple one-dimensional system correspond to closed or periodic orbits in the full two-dimensional system. Assuming that Ω_b is about 1.85 times the angular rotation rate at the solar circle (Dehnen 1999) and a flat rotation curve, we estimate $\bar{\delta} \sim 0.05$ at the solar circle. This drops to zero as we approach the 2 : 1 OLR_B, at a Galactocentric radius of $r \approx 0.9 r_0$. Because $a' \sim -5.7/r_c^2$, $\bar{\beta} \sim -0.2\beta_2 r_c/v_c^2$ and $\bar{\epsilon} \sim -0.2\epsilon_m r_c/v_c^2$. For radii outside the OLR_B, $\bar{\delta} > 0$ and we expect only one fixed point or periodic orbit. Because $\bar{\beta} > 0$, the quasi-periodic orbits at the solar circle, outside the OLR_B, will be aligned with the bar. They are referred to as the $x_1(1)$ orbits (see, e.g., Fux 2001; Dehnen 2000). Inside the OLR_B, the resonance bifurcates and two families of periodic orbits (fixed points) exist, the $x_1(1)$ and $x_1(2)$ families. The $x_1(2)$ family is aligned perpendicular to the bar and found at $\phi = \pi$. We expect that large-scale chaos can occur when there is a separatrix, $\bar{\delta} < 0$, and inside the radius of the OLR_B.

The quantity Ω_s is $\sim$0.3 times the angular rotation rate at the solar circle when r_0 is just outside the 2 : 1 ILR_S, and 0.6 if r_0 is just within the 4 : 1 ILR_S. The quantity γ is related to the phase of the potential for the spiral pattern. For spiral structure at our location in the solar neighborhood, we should be outside the m : 1 ILR_S of the pattern, so that $\Delta < 0$. If we are not outside the resonance, the stellar orbits will not support the spiral structure and will negate it instead (e.g., Contopoulos 1988). Inside the ILR_S there is only one periodic orbit or fixed point, and the resonance bifurcates outside the ILR_S (see Figs. 1 and 2 of Contopoulos 1975). We expect $\bar{\epsilon} < 0$, so that periodic orbits with $\phi = \gamma$ would be in phase with the spiral arm. By "in phase," we mean that the orbit will be aligned with radial maxima on the same axis as the density maxima.

3.1. *Generating Poincaré Maps*

Previous works addressing the stability of orbits in the solar neighborhood have computed Lyapunov exponents, studied N-body simulations (Fux 2001), or carried out backward-integration schemes (Dehnen 2000). Here we adopt the approach of Fux (2001) and strive to identify regions of phase space that can keep stars for long periods of time. However, as we explain below, we do this by determining which regions of phase space are filled with area-filling, or chaotic, orbits rather than computing Lyapunov exponents.

The Hamiltonian (eq. [23]) contains two main resonant terms separated by a frequency $\bar{\nu}$. This is similar to the forced pendulum. When the two resonances overlap, a chaotic region can be generated at the separatrix of one of the resonances. For a fully overlapped system, this zone has a Lyapunov time $\sim 2\pi/\bar{\nu}$, corresponding to the separatrix pulsation period (Holman & Murray 1996). Outside the main chaotic zone, we expect quasi-periodic islands. This picture is qualitatively different from that explored by Fux (2001), who illustrated narrow bands of unstable regions, each with different Lyapunov timescales. We expect instead large bands of chaos described by one Lyapunov time that are surrounding stable islands. Consequently, we do not compute Lyapunov times for a range of initial conditions but instead map the structure of the phase space itself.

To investigate the stability of the system containing perturbations from both the bar and spiral structure, we numerically integrate the equations of motion determined from the Hamiltonian given by equation (23). This system is time-dependent, so the Hamiltonian itself is not conserved. However, if we plot points every time step $P_\nu = 2\pi/\bar{\nu}$, we derive an area-preserving, or Poincaré, map. This procedure generates maps that are like surfaces of section, and these we can use to study the stability of the orbits. In such a map, orbits are either area-filling or curves. We denote area-filling orbits as chaotic (in the sense that orbits diverge exponentially) and the curved orbits as quasi-periodic.

This procedure is excellent for addressing the question of orbit stability and identifying the regions accessible to individual orbits. But because we plot every P_ν, we cannot tell whether an orbit is librating around ϕ or around an angle $\phi + \bar{\nu}t$. This makes it difficult to determine whether fixed points are associated with (or supporting) the bar or the spiral pattern. However, we can qualitatively deal with this problem by changing the orientation of the spiral perturbation. We do this by adjusting γ, which determines the relative phase of the bar with respect to the spiral pattern at time $t = 0$. To make our Poincaré maps, we plot points every P_ν; however, we could choose our initial time to be anywhere between 0 and P_ν without changing the topology of the map. This is equivalent to changing γ as long as the bar pattern speed is an irrational number times the spiral pattern speed. We set $\gamma = \pi/2$ so that orbits in phase with the spiral pattern are located at an angle of $\phi \sim \pi/2$. Orbits perpendicular to the spiral pattern are located at an angle of

$-\pi/2$. In comparison, orbits associated with the bar's OLR_B librate about $\phi = 0$ or $\phi = \pi$.

As is commonly done, (e.g., Murray & Dermott 1999; Borderies & Goldreich 1984), we plot all figures in this paper in a coordinate system with

$$x = \sqrt{2j_1}\cos\phi\ , \quad y = \sqrt{2j_1}\sin\phi\ . \tag{28}$$

With respect to our action variable, $j_1 = s^2/2$, where s is the radial distance on these plots. Since we defined $J_1 = j_1\Omega r_c^2$, the epicyclic amplitude is approximately the same as s, the radial distance in these plots. In other words, s gives the maximum difference between the radial position of a particle and r_c (see eq. [2]).

For each series of integrations (Figs. 2–4), we assume a value for Ω_s and Ω_b (in units of the solar neighborhood angular rotation rate Ω_0) and $\bar{\epsilon}$ and $\bar{\beta}$, which are directly estimated from the strengths of the spiral structure and bar (see previous sections). We define the radial offset dr from the radius of the Sun as

$$dr = (r_0 - r_c)/r_c\ , \tag{29}$$

so that $\Omega_0/\Omega = r_c/r_0 = 1 + dr$. The values of $\bar{\delta}$ and $\bar{\nu}$ for each integration are calculated from Ω_s and Ω_b, assuming a flat rotation curve and for a range of dr. In the figures, the different panels correspond to different values of dr.

Both the spiral and bar resonances have the topology illustrated in Figure 1. Considering the bar only, as we vary the radius, or dr and so $\bar{\delta}$, phase space changes in appearance from that shown at the top of Figure 1 to that in the bottom of this figure as we pass through the OLR_B. Considering the spiral arms only, phase space from this resonance should look like the bottom of Figure 1 but rotated by 90°, since we chose $\gamma = \pi/2$. Now we consider what happens when both resonances are present. In this case, the bar resonance (which could be any of the three panels shown in Fig. 1) overlaps the spiral resonance (a panel looking like the bottom of Fig. 1). When $\bar{\delta} < 0$, the bar OLR_B gains a separatrix that is likely to become unstable when perturbed by the spiral arms.

In Figure 2, we show the result of integrating equation (23) for a two-armed pattern near the 4 : 1 ILR_S of the spiral pattern for moderate spiral and bar strength. For each of 30 particles chosen with different initial conditions, 200 time steps are plotted with $dt = 2\pi/\nu$. For the panel on the top left, corresponding to the Galactic radius of the Sun, the orbits librate about $\phi = \pi/2$ and support the spiral structure. At $dr \sim -0.10$, orbits become are aligned with the bar [$x_1(1)$-type orbits] and librate about $\phi = 0$. At $dr = -0.13$, the $x_1(2)$ orbits appear. These librate about $\phi = -\pi$ and are oriented perpendicular to the bar. As dr decreases further, the orbits librate closer and closer to $\phi = \pi/2$ and so support the spiral structure and are no longer aligned perpendicular to the bar.

Just past the OLR_B (the center of the resonance is near $\delta = 0$, but a separatrix appears only for negative values of δ), we see in Figure 2 that the quasi-periodic regions are bounded by thick bands of area-filling or chaotic orbits. The spiral structure is disrupted (unsupported) between $dr = -0.11$ and $dr = -0.15$. Past $dr = -0.175$, the $x_1(2)$ orbits are limited by the influence of the spiral structure. In short, the spiral structure limits the extent of the orbits perpendicular to the bar, and the bar's OLR_B disrupts the spiral structure over a narrow range of radius.

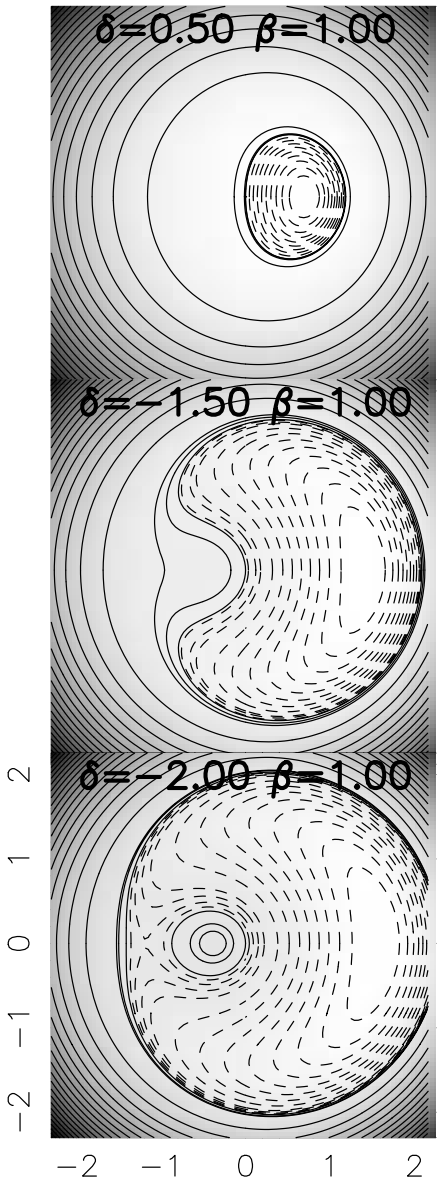

FIG. 1.—Level contours of the Hamiltonian $H(j, \phi) = j^2 + j\bar{\delta} - \bar{\beta}j^{1/2}\cos\phi$. Dashed contours are negative. The axes (x, y) are defined by eq. (28). The critical value for the resonance to bifurcate happens in the middle panel, where $\frac{2}{3}\bar{\delta}/|\bar{\beta}|^{2/3} = -1$. The top panel contains a fixed point, which would correspond to a closed or periodic orbit aligned with the bar, so that $\phi = 0$. This is the situation outside the OLR_B. Inside the OLR_B the resonance bifurcates, and both periodic orbit families are present. This situation is shown in the bottom panel. The fixed points at $\phi = \pi$ correspond to periodic orbits oriented perpendicular to the bar. Only when $\frac{2}{3}\bar{\delta}/|\bar{\beta}|^{2/3} < -1$ is there a separatrix. Additional perturbations are most likely to cause instability when there is a separatrix. Changing the sign of β is equivalent to adding π to ϕ. The Lindblad resonances associated with spiral arms have the same structure, though outside the ILR_S the resonance looks like the bottom panel, and two classes of closed or periodic orbits exist. Inside the ILR_S the resonance looks like the top panel, and only one class of periodic orbits exists.

3.2. *On the* (u, v)*-Plane*

To see whether our maps correspond to what is observed in the local velocity distribution, we must consider what values of our action angle variables correspond to the (u, v)-velocities that are used to measure stars in the solar neighborhood.

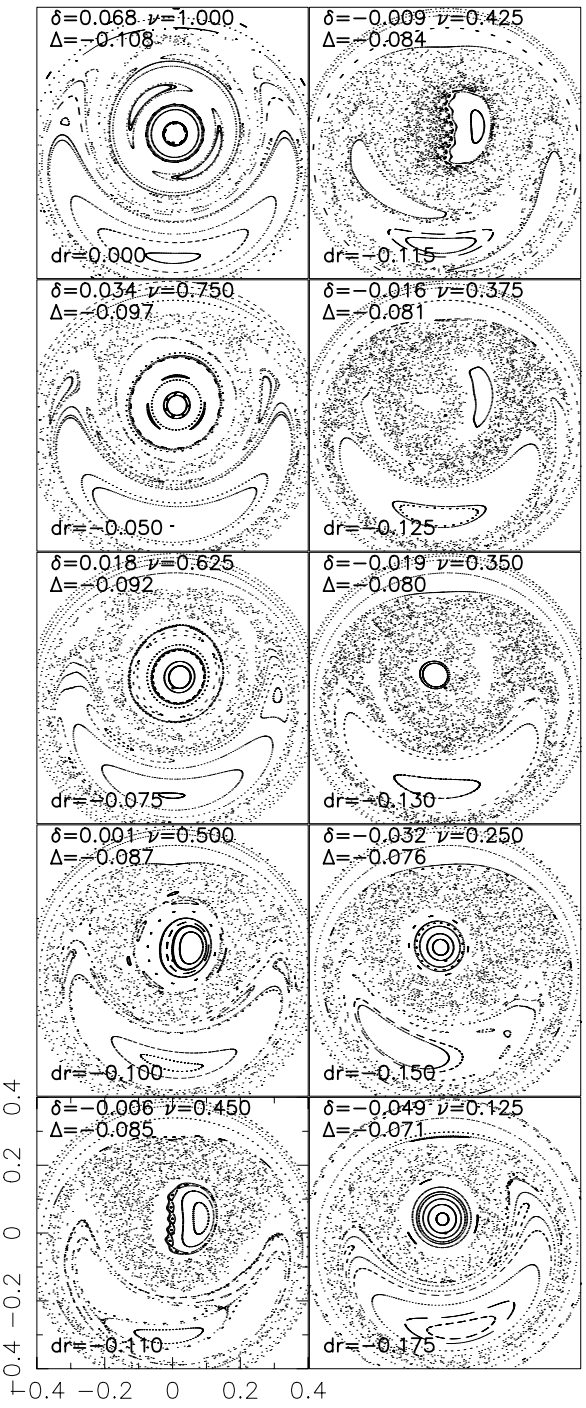

FIG. 2.—Poincaré maps made by integrating the Hamiltonian of eq. (23) with $m = 2$ and with a time step of $2\pi/\bar{\nu}$. The panels are at different values of dr. The top left panel has the smallest value of dr, corresponding to a location near the solar neighborhood. The bottom right panel has the most negative value of dr, corresponding to a radius closer to the Galactic center. All panels have the same values of $\bar{\epsilon}$ (=−0.004), describing the strength of spiral structure, Ω_s (=0.60), the pattern speed of the spiral structure in units of the solar neighborhood angular rotation rate (Ω_0), $\bar{\beta}$ (=0.0006), describing the strength of the bar, and Ω_b (=1.90), the pattern speed of the bar in units of Ω_0. Phase space, as illustrated by the structure in these maps, has two types of orbits; curved linear structures, corresponding quasi-periodic orbits, and area-filling orbits, corresponding to chaotic regions. The radial distance on these plots is approximately the same as the radial epicyclic amplitude in units of r_0, or the distance the orbit reaches from r_c. A dot is placed at the origin for reference. The spiral pattern speed considered here would result from a two-armed spiral pattern with the solar neighborhood just within the 4 : 1 ILR_S.

The solar neighborhood velocity distribution is typically plotted with respect to the azimuthal velocity component v and the radial velocity u, where $u > 0$ corresponds to velocities toward the Galactic center. We define v such that the tangential component of the velocity, in the direction of Galactic rotation, is equal to $v_c + v$. An orbit at a lower v should have a lower r_c value and so should oscillate about a Galactic radius that is smaller than r_0, the radius of the solar circle. We now estimate what values of dr correspond to the center and boundary of the Hercules Stream, or u-anomaly.

If we assume a flat rotation curve, the Hamiltonian lacking nonaxisymmetric perturbations is given by

$$\frac{H}{v_c^2} = \frac{u^2}{2v_c^2} + \frac{(v_c + v)^2}{2v_c^2} + \ln\left(\frac{r}{r_0}\right) . \tag{30}$$

For a circular orbit of radius r_c, both u and v are zero and

$$H/v_c^2 = \tfrac{1}{2} + \ln(r_c/r_0) . \tag{31}$$

We set $r = r_0$ at the solar neighborhood, equate the two expressions, and solve for r_c as a function of the tangential velocity component v, finding $\ln(r_c/r_0) = (v/v_c) + \frac{1}{2}(u^2 + v^2)/v_c^2$. We expand $\ln(r_c/r_0)$ and obtain

$$dr \approx \frac{v}{v_c} + \frac{v^2 + u^2}{2v_c^2} . \tag{32}$$

Note that we have not included the bar or spiral perturbation in our estimate of dr. This dr is valid as long as the above estimate is greater than β_2/v_c^2 and A_2/v_c^2. We expect these to be satisfied for moderate values of v, and for velocities associated with the Hercules Stream (see eqs. [8] and [13]).

Assuming $u = 35$ km s^{-1} at the center of the stream and $v_c = 220$ km s^{-1},

$$dr \sim \begin{cases} -0.13 , & \text{for } v \sim -30 \text{ km s}^{-1} , \\ -0.18 , & \text{for } v \sim -45 \text{ km s}^{-1} , \end{cases} \tag{33}$$

where $v \sim -45$ km s^{-1} at the center of the Hercules Stream or u-anomaly and $v \sim -30$ km s^{-1} at the edge or boundary of the stream.

The stream itself is quite wide along the u-direction (over 100 km s^{-1} wide) and comparatively quite narrow in the v-direction (40 km s^{-1} wide). In fact, the mean u-value of the stream is much less than its u-width. If we use a width in u of 35 ± 50 km s^{-1}, then we estimate a range of $-0.21 \lesssim dr \lesssim -0.07$ in the stream.

In Figure 2, we have chosen the bar pattern speed so that the $x_1(2)$ OLR_B orbits appear near $dr \sim -0.15$, which is approximately at the location of the Hercules Stream or u-anomaly. We could adjust the pattern speed of the bar to move the location of these orbits. Equation (26) could be used to constrain the pattern speed and bar strength. However, before we do this we should consider the approximations made in our analysis. In the full Hamiltonian given in equation (17), there is a term proportional to $J_1 J_2$, which, had we kept it in our analysis, would have caused an additional term $(b'/a')J_2/(\kappa_c r_c^2)$ added to $\bar{\delta}$ in equation (23). In dropping the extra terms in the Hamiltonian, we have assumed that J_2 is small. Because b' is the same sign as a', δ should be larger than we have calculated. This would have the effect of shifting the location of the resonance to more negative dr, or larger distances from the solar neighbor-

hood. Note that if the rotation curve is not flat, then the location of the resonance would also shift.

The maps shown in Figures 2–4 do show the likely morphology of phase space near the OLR$_B$. However, we should not use them to constrain the bar pattern speed at a level better than 25% unless we have taken into account this correction and quantified our uncertainties in the shape of the rotation curve.

To find out whether stars in orbits associated with the $x_1(2)$ family can reach the solar neighborhood, we also need to estimate the size of our action variable for the *u*-anomaly. If we assume that $u \sim 0$, then the epicyclic amplitude is set by the condition that we are at r_0. In other words, the maximum value in $r - r_c$ is approximately $r_0\, dr$. In terms of the coordinate system of our Poincaré maps, a star that reaches the solar neighborhood has $s \sim dr$.

In Figure 2, for $dr \sim -0.15$ the quasi-periodic regions are of size $s \sim 0.17$, which exceeds the value of dr. This is large enough that stars in these orbits would reach the solar neighborhood. For $dr \lesssim 0.125$, no $x_1(2)$ orbits exist and no stellar orbits aligned perpendicular to the bar will reach the solar neighborhood. Because each value of dr is associated with a v-value in the solar neighborhood velocity distribution, this implies that above a particular value of v no orbits can be in the quasi-periodic orbit region surrounding the $x_1(2)$ periodic orbits. Our model predicts that the *u*-anomaly should have a sharp boundary in v in the solar neighborhood velocity distribution, as observed. A model lacking spiral structure would predict this sharp edge as well, since it is determined by the value of δ at which the resonance bifurcates (see Fig. 1, the condition given in eq. [26]).

In Figure 2, we see that past a certain value of dr, corresponding to a value of v, the quasi-periodic orbits are more likely to be oscillating with the spiral structure than the bar. This implies that there should be a smoother upper boundary in v to the Hercules Stream or *u*-anomaly.

We see in Figure 2 that the quasi-periodic orbits oriented perpendicular to the bar are bounded by chaotic regions. This implies that there is a limit in the extent of the epicyclic amplitude of stars associated with this quasi-periodic region. In the solar neighborhood, this implies that there would be a maximum value of *u* for orbits in the *u*-anomaly. Since stars in the chaotic regions can rapidly achieve very different epicyclic amplitudes, the boundaries of the *u*-anomaly are probably set by the extent of the quasi-periodic orbits associated with the $x_1(2)$ orbits.

3.3. *Changing the Spiral Pattern Speed*

According to Contopoulos (1988) and Patsis & Kaufmann (1999), two-armed spiral structure should only extend between its 2 : 1 and 4 : 1 ILR$_S$'s. These works showed that two-armed spiral structure was not supported by the stellar orbits past the 4 : 1 ILR$_S$. At first we consider pattern speeds that are faster and, so, with the solar neighborhood nearer the 2 : 1 ILR$_S$. The result of integrating equation (23) with a faster pattern, $\Omega_s = 0.45$, in units of the solar angular rotation rate Ω_0, is shown in Figure 3. This pattern speed would be consistent with a two-armed spiral pattern near its 2 : 1 ILR$_S$.

In Figure 3, we see large-scale chaotic regions that completely disrupt the spiral structure and the orbits associated with the OLR$_B$. Because $\bar{\nu}$ is smaller in this integration than that shown in Figure 2, the resonances are closer together

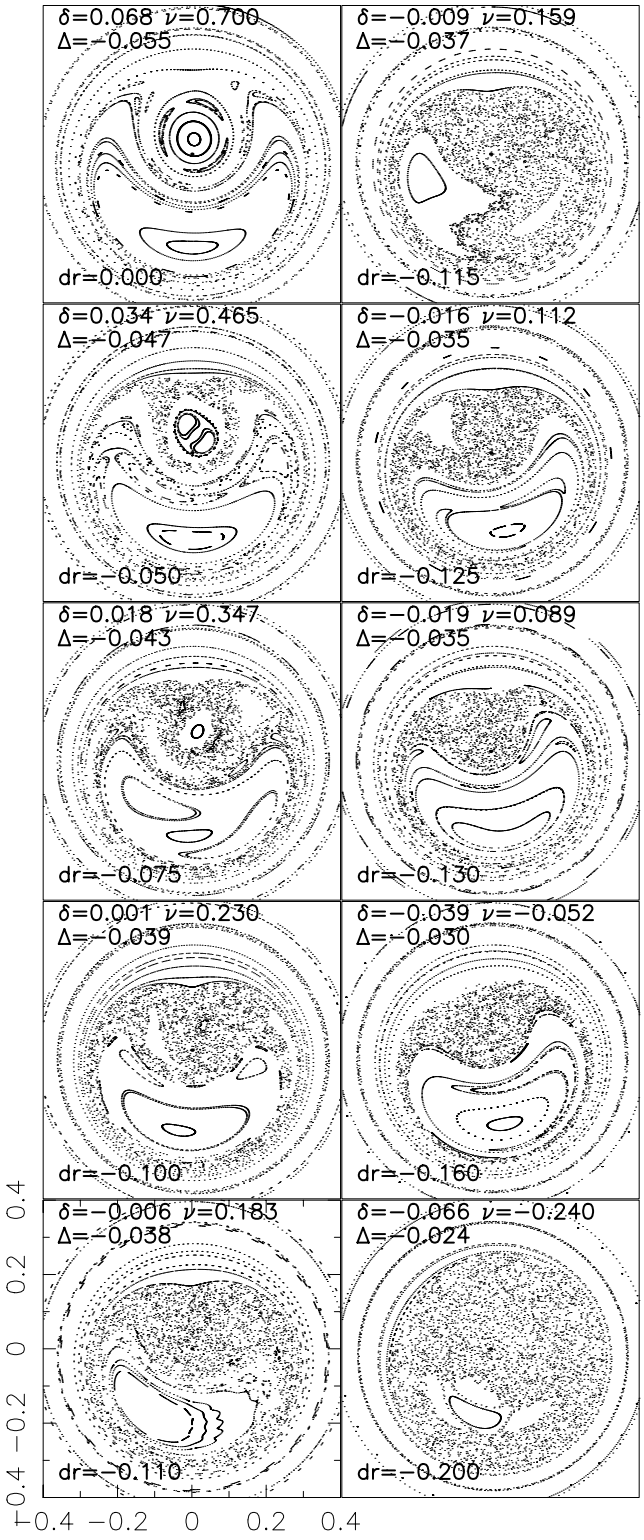

FIG. 3.—Similar to Fig. 2, but we have changed the pattern speed of the spiral structure to $\Omega_s = 0.45$ (all panels have $\bar{\epsilon} = -0.004$ and $\bar{\beta} = 0.0005$). This pattern speed could result from a two-armed spiral pattern with the solar neighborhood fairly near the 2 : 1 ILR$_S$. Since $\bar{\nu}$ is smaller, the resonances are more fully overlapped than is the case in Fig. 2. Both the spiral structure and resonant orbits at the OLR$_B$ are disrupted. A resonant island of $x_1(2)$ orbits does not exist for $\Omega_s \lesssim 0.5$ for bar and spiral arm strengths estimated from observations of the stellar density variations.

and so more fully overlapped. The scale of the chaotic regions can be reduced by decreasing the strength of the bar and spiral perturbations, or the values of $\bar{\epsilon}$ and $\bar{\beta}$. However, decreasing both $\bar{\epsilon}$ and $\bar{\beta}$ by a factor of 2 does not restore the quasi-periodic island about the $x_1(2)$ family of periodic orbits. The scale of the chaotic zone is more sensitive to the extent the resonances overlap or to $\bar{\nu}$, which is set by the spiral pattern speed, than to the size of the perturbations. Since we have adopted realistic values for the bar and spiral arm strength, we can use this sensitivity to place an approximate limit on the pattern speeds of spiral structure that passes through the OLR_B. We find that the $x_1(2)$ orbits are completely disrupted for $\Omega_s \lesssim 0.45$, implying that two-armed spiral structure passing through the OLR_B is likely to be rotating faster than this.

In Figure 4, we have integrated a spiral pattern at a faster pattern speed of $\Omega_s = 0.85$ for $m = 4$. This would correspond to a four-armed spiral pattern. The situation is similar to that seen in Figure 2. The OLR_B disrupts the spiral pattern on the outer side of the resonance. The $x_1(2)$ orbit family appears abruptly at $dr \sim -0.13$, and the quasi-periodic island oscillates with the bar until $dr \sim -0.15$, where it is destroyed along with orbits that support the spiral structure.

If we reduce the pattern speed of four-armed spiral structure to $\Omega_s < 0.75$, phase space looks like that shown in Figure 3. Both the $x_1(2)$ orbit family and quasi-periodic orbits that support the spiral structure are destroyed. This implies that four-armed spiral structure faster than $\Omega_s = 0.75$ cannot pass through the OLR_B.

4. SUMMARY AND DISCUSSION

In this paper, we have considered the dynamics of stars that are affected by perturbations from both spiral structure and the Milky Way bar. We constructed a simple one-dimensional Hamiltonian model for the strongest resonances in the epicyclic action and angle variables.

This Hamiltonian is time-dependent because the bar and spiral structure in general have different pattern speeds, and it resembles a forced pendulum. To address the issue of orbit stability and differentiate between areas of phase space filled with quasi-periodic orbits and area-filling, or chaotic, orbits, we numerically integrated this Hamiltonian. By plotting points only at the period that separates the two resonant perturbations, we construct Poincaré maps that illustrate where in phase space there are area-filling or chaotic orbits instead of quasi-periodic orbits.

The Lyapunov time in the chaotic regions is on the order of the period that separates two resonances (Holman & Murray 1996). Over much of the resonance, this timescale is on the order of a few times the rotation period. Consequently, stars that are located in chaotic regions can move across the region. This implies that they can achieve large epicyclic amplitudes and will not remain in any coherent, small region in phase space. Streams seen in the local velocity distribution are unlikely to be located in large chaotic regions. In contrast, particles that are located in quasi-periodic regions should maintain their epicyclic amplitudes for much longer times. Our model predicts that the chaotic regions can form large bands. This is a qualitatively different picture from the narrow regions spanning a range of Lyapunov times illustrated by Fux (2001), who solely considered perturbations from the bar.

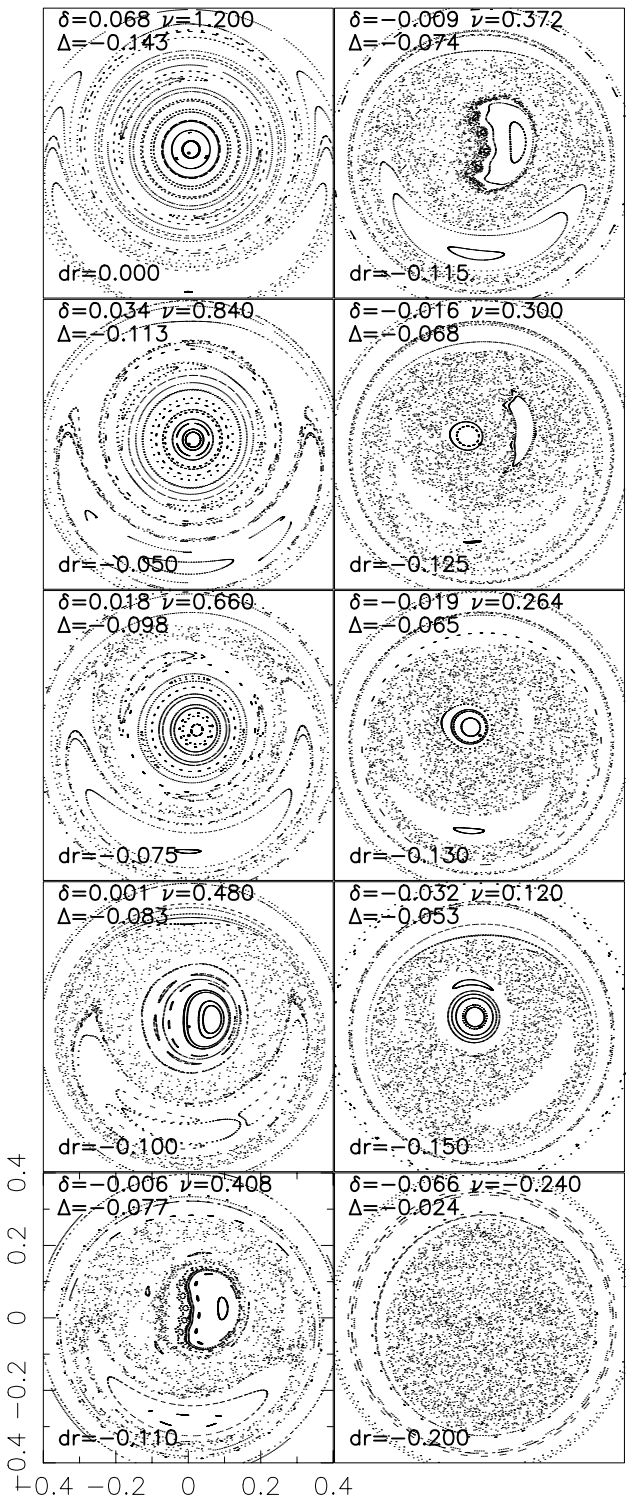

FIG. 4.—Similar to Fig. 2, but we have changed the pattern speed of the spiral structure to $\Omega_s = 0.85$, with the solar neighborhood outside the 4 : 1 ILR_S (all panels have $\bar{\epsilon} = -0.002$). For this simulation $m = 4$, corresponding to a weak four-armed spiral pattern. Quasi-periodic orbits exist near the solar circle (dr small) associated with the spiral structure. Around $dr = 0.125$, the $x_1(2)$ family of orbits oriented perpendicular to the bar appears. Past $dr = -0.20$ no low-amplitude quasi-periodic orbits associated with either bar or spiral structure exist. The spiral structure is not strong enough to disrupt the orbit families near the bar, but also not strong enough to persist inside the OLR_B. For faster pattern speeds, the family of orbits perpendicular to the bar associated with the OLR_B is entirely disrupted.

We note that the diffusion timescale in a chaotic region is not the same as the Lyapunov time. The diffusion timescale should depend on the size of the perturbations and should be longer than the Lyapunov time (see, e.g., discussion in Murray & Holman 1997). Further work would be required to explore heating of the stellar disk resulting from perturbations at different pattern speeds.

We find that faster spiral pattern speeds cause less overlap in the two resonances and, so, smaller chaotic zones. Spiral structure at a pattern speed that puts the solar circle near the 2 : 1 ILR_S produces extremely large bands of chaos near the 2 : 1 OLR_B with the bar. This disrupts the spiral pattern and destroys orbits perpendicular to the bar near the OLR_B. It is unlikely that two-armed spiral structure at patterns slower than $\Omega_s = 0.5$ extends into the OLR_B. Likewise, it is unlikely that a four-armed spiral slower than $\Omega_s = 0.85$ extends into the OLR_B. It is possible that the OLR_B forms a boundary between spiral structures at different pattern speeds.

Two-armed and four-armed spiral structures at faster pattern speeds are much less disruptive. For a two-armed pattern with $\Omega_s = 0.6$, chaotic regions appear near the OLR_B that disrupt the spiral pattern only across a narrow region. Orbits oriented perpendicular to the bar appear at tangential velocities and epicyclic amplitudes consistent with the existence of quasi-periodic or stable orbits in the local velocity distribution at the Hercules Stream, or *u*-anomaly. The boundaries of the *u*-anomaly are set by the extent of the quasi-periodic orbits associated with the family of orbits perpendicular to the bar.

In this paper, we have considered the combined problem of a resonance from spiral structure and from a Galactic bar. Notably, the solar neighborhood contains a wealth of structure at smaller velocities than the *u*-anomaly (Dehnen 1998). Much of this structure contains old stars and so is likely to be caused by spiral structure. Since there is more than one clump in the distribution, it is likely that the solar neighborhood is influenced by spiral structure at more than one pattern speed. Hence we expect complicated phenomena such as that discussed here. In future work we will concentrate on the interplay between different modes of spiral structure.

4.1. *Caveats*

Our simple Hamiltonian model assumes that the value of r_c is constant. There is no canonical transformation showing us how to pick r_c, a serious problem with our choice of action angle variables. By working with the perturbative approach of Contopoulos (1975), we have assumed that all orbits oscillate about a given radius. We have also neglected coupling between the two degrees of freedom (the term proportional to $J_1 J_2$ in eq. [17]). While our simplified model is likely to qualitatively illustrate chaos caused by resonance overlap when multiple resonances are present, it will not illustrate other phenomena that would be present in the entire two-dimensional system. For example, particles integrated numerically in a system with both spiral structure and a bar can drift in both angular momentum and energy, so that a mean radius may not be preserved.

This work could not have been carried out without helpful discussions with Larry Helfer and Don Garnett. A. C. Q. gratefully thanks the Technion for hospitality and support during the fall of 2001.

REFERENCES

Binney, J., & Tremaine, S. 1987, Galactic Dynamics (Princeton: Princeton Univ. Press)
Borderies, N., & Goldreich, P. 1984, Celest. Mech., 32, 127
Contopoulos, G. 1975, ApJ, 201, 566
———. 1988, A&A, 201, 44
Dehnen, W. 1998, AJ, 115, 2384
———. 1999, ApJ, 524, L35
———. 2000, AJ, 119, 800
Drimmel, R., & Spergel, D. N. 2001, ApJ, 556, 181
Dwek, E., et al. 1995, ApJ, 445, 716
Fux, R. 2001, A&A, 373, 511
Gerhard, O. 2002, in ASP Conf. Ser. 273, The Dynamics, Structure and History of Galaxies ed. G. S. Da Costa & H. Jerjen (San Francisco: ASP), 73
Holman, M. J., & Murray, N. W. 1996, AJ, 112, 1278
Holmberg, J., & Flynn, C. 2000, MNRAS, 313, 209
Murray, C. D., & Dermott, S. F. 1999, Solar System Dynamics (Cambridge: Cambridge Univ. Press)
Murray, N., & Holman, M. 1997, AJ, 114, 1246
Patsis, P. A., & Kaufmann, D. E. 1999, A&A, 352, 469
Raboud, D., Grenon, M., Martinet, L., Fux, R., & Udry, S. 1998, A&A, 335, L61
Skuljan, J., Hearnshaw, J. B., & Cottrell, P. L. 1999, MNRAS, 308, 731
Vallée, J. P. 1995, ApJ, 454, 119
Weinberg, M. D. 1994, ApJ, 420, 597